Biophysical Journal
Article

# Nanoscale membrane curvature sorts lipid phases and alters lipid diffusion

Xinxin Woodward,[1] Matti Javanainen,[2,3] Balázs Fábián,[2] and Christopher V. Kelly[1,*]
[1]Department of Physics and Astronomy, Wayne State University, Detroit, Michigan; [2]Institute of Organic Chemistry and Biochemistry, Czech Academy of Sciences, Prague, Czech Republic; and [3]Institute of Biotechnology, University of Helsinki, Helsinki, Finland

ABSTRACT The precise spatiotemporal control of nanoscale membrane shape and composition is the result of a complex interplay of individual and collective molecular behaviors. Here, we employed single-molecule localization microscopy and computational simulations to observe single-lipid diffusion and sorting in model membranes with varying compositions, phases, temperatures, and curvatures. Supported lipid bilayers were created over 50-nm-radius nanoparticles to mimic the size of naturally occurring membrane buds, such as endocytic pits and the formation of viral envelopes. The curved membranes recruited liquid-disordered lipid phases while altering the diffusion and sorting of tracer lipids. Disorder-preferring fluorescent lipids sorted to and experienced faster diffusion on the nanoscale curvature only when embedded in a membrane capable of sustaining lipid phase separation at low temperatures. The curvature-induced sorting and faster diffusion even occurred when the sample temperature was above the miscibility temperature of the planar membrane, implying that the nanoscale curvature could induce phase separation in otherwise homogeneous membranes. Further confirmation and understanding of these results are provided by continuum and coarse-grained molecular dynamics simulations with explicit and spontaneous curvature-phase coupling, respectively. The curvature-induced membrane compositional heterogeneity and altered dynamics were achieved only with a coupling of the curvature with a lipid phase separation. These cross-validating results demonstrate the complex interplay of lipid phases, molecular diffusion, and nanoscale membrane curvature that are critical for membrane functionality.

SIGNIFICANCE Nanoscopic membrane organization and dynamics are critical for cellular function but challenging to experimentally measure. This work brings together super-resolution optical methods with multiscale computational approaches to reveal the interplay between curvature, composition, phase, and diffusion in model membranes. Nanoscale membrane curvature induced phase separation in otherwise homogeneous membranes, and the phase-curvature coupling had a direct implication on lipid mobility. This discovery advances understanding of the fundamental membrane biophysics that regulate membrane activities such as endocytosis and viral budding.

## INTRODUCTION

Cell plasma membranes contain thousands of distinct lipid species with spatial heterogeneity in composition and shape. Natural membrane compositions near a phase coexistence manifest functional membrane domains that are more and less structured and resemble liquid-ordered ($L_o$) and liquid-disordered ($L_d$) phases (1–4). Membrane domains are critical for cell functions such as protein sorting, cell signaling, membrane budding, and retrovirus replication through the regulation of local variations in the membrane composition (4–8). Caveolae, for example, are cholesterol- and sphingolipid-rich endocytic buds that have diverse roles in membrane compositional regulation, trafficking, force sensing, and endocytosis on the sub-100-nm-length scale (9–11). The coupling of membrane phases and curvature on live cells remains unconfirmed yet crucial for diverse cellular functions.

Model membranes of known lipid mixtures provide a means to reveal how the membrane composition affects function. Coexisting $L_o$ and $L_d$ phases can be created by combining a sterol, a phospholipid with a high chain-melting temperature, and a phospholipid with a low chain-melting temperature below the mixture's miscibility transition temperature ($T_{mix}$) (12,13). Phase-separated model membranes have shown curvature-dependent phase separations in tubules (14–17), small vesicles (18), and supported lipid bilayers (SLBs) (19–21). In select cases, the membrane shape

Submitted August 18, 2022, and accepted for publication January 3, 2023.
*Correspondence: cvkelly@wayne.edu
Editor: Antje Pokorny Almeida.
https://doi.org/10.1016/j.bpj.2023.01.001

has been shown to induce a phase separation that was not observed on planar membranes (14,15). In model membranes, the region of greater curvature (i.e., smaller radius) concentrates disordered lipids as the $L_d$ phase has a lower bending rigidity than the $L_o$ phase (22). Interestingly, however, endocytic processes and viral budding in live cells are typically correlated with $L_o$-preferring lipids, such as cholesterol and sphingomyelin (23), which may occur if the area of the ordered phase is significantly smaller than the disordered phase or if the order-preferring lipids and proteins have a greater spontaneous curvature (24). Typically, single lipids are too small relative to the membrane curvature for the curvature to significantly alter their distribution in the membrane without the collective action of lipid phases (18,25–27). The physical principles that govern the sorting of lipids to <100-nm-membrane buds remain a mystery fundamental to both cellular homeostasis and pathophysiology. This article reports the temperature-dependent diffusion and sorting on membranes to better understand the interplay of lipid mobility, phase separation, and curvature.

Lipid diffusion in the $L_d$ phase is up to 10 faster than lipids in the $L_o$ phase, depending on the membrane composition, the fluorescent lipids tracked, and the substrate topography (28–33). For example, DPPE-Texas Red in SLBs composed of DiPhyPC, DPPC, and cholesterol at molar ratios of 2:2:1 had a diffusion coefficient (1.8 5 0.5) greater in the $L_d$ phase than in the $L_o$ phase (34). The diffusion in the two phases became indistinguishable when the sample is near or above $T_{mix}$, which can occur with increasing the temperature or cholesterol content, as is associated with shorter tie lines separating the phases. For example, SLBs composed of DiPhyPC, DPPC, and cholesterol at molar ratios of 1:1:2 demonstrated lipid phase separation, as evident by the partitioning of DPPE-Texas Red, but no difference in the DPPE-Texas Red diffusion was observed between the two phases (34).

Experimental limitations and the underlying topological manifold result in the motion of particles on curved membranes appearing non-Brownian (35). Restrictions on the observable lag times and localizations precision result in the measured diffusion becoming increasingly nonlocal in the sense that observed particle motion averages patches of the membrane. Consequently, the lipid mobility becomes reflective of the average membrane environment with a loss of nanoscale information. Nonetheless, modern single-particle localization and computational methods are converging to reveal spatially varying membrane behaviors at physiological length scales.

The influence of membrane curvature on single-lipid diffusion has been studied in well-defined geometries. Diffusion typically slows on cylindrical membranes when the radii are smaller than 50 nm (36), but the effects of curvature on lipid diffusion are correlated to the fluorophore location on the labeled lipid; head-group-labeled lipids diffuse 3 faster on flat versus curved membranes, whereas tail-labeled lipids diffuse at the same rate on flat and curved membranes (37). Recent experimental and computational capabilities to measure diffusion and sorting at the nanoscale are beginning to reveal an intertwined network of contributing factors affecting membrane phenomena, including the effects of hydrodynamics, geometry, projection, lipid packing, and measurement time. For example, membrane curvature affects the thickness, area per lipid, and the order parameter of the lipid hydrocarbon chains (38).

In this article, the diffusion and sorting of lipids relative to nanoscale membrane curvature and phase separation are quantified with experimental and computational methods. Single-component membranes displayed negligible changes to the local membrane composition or dynamics relative to membrane curvature (Fig. 1, A and B). Membranes of mixed composition demonstrated sorting of an $L_d$ phase to the nanoscale curvature regardless of if the planar membrane was above or below $T_{mix}$ (Fig. 1, C–E). These results were observed experimentally and computationally by fluorophore sorting, single-lipid diffusion, coarse-grained molecular dynamics, and continuum simulations. Membrane curvature was experimentally generated by creating phase-separated SLBs over 50-nm-radius nanoparticles on planar microscopy coverslips (Fig. 2). The concentration of DPPE-Texas Red on the curved membrane was measured via diffraction-limited images and analyzed for lipid sorting. Single-molecule localization microscopy and single-particle tracking (SPT) were performed to track individual DPPE-Texas Red molecules and to measure their curvature- and phase-dependent mobility. The disorder-preferring fluorescent lipids were more concentrated on the curved membrane than the surrounding planar bilayer when embedded in a membrane capable of sustaining lipid phase separation. This sorting occurred regardless of the phase of the immediately surrounding bilayer, but sorting was more pronounced if the membrane bud was immediately surrounded by a $L_o$ phase. The single-lipid diffusion was up to 2.2 faster on curved versus planar membranes, with a dependence on the length of the phase-separating tie-lines. These experimental results were verified in computational simulations of phase separation, including continuum and molecular dynamics simulations with explicit or spontaneous phase-curvature coupling, respectively. The sorting of disorder-preferring lipids to the curvature and the effects of the curvature propagating onto the surrounding planar membrane were consistently observed with the curvature site acting to seed lipid phase separation for larger-scale influence over the surrounding membrane's average phase. Further, the sorting of the lipid phases to curvature sites occurred even when the sample conditions (i.e., composition and temperature) were such as to not induce large-scale phase separation on the planar membrane. This

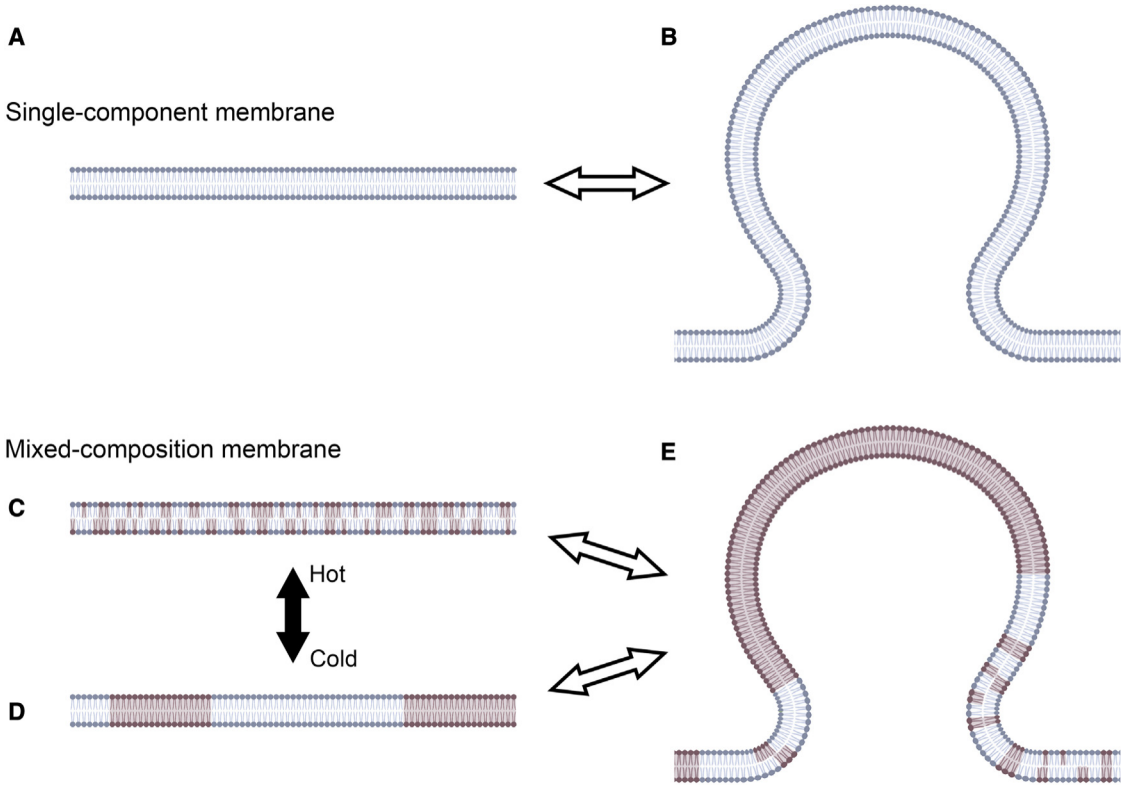


FIGURE 1 (A and B) Single-component membranes have no apparent redistribution of fluorescent lipids and minimal or fluorophore-dependent curvature dependence on the single-lipid diffusion. (C–E) Membranes of mixed composition, however, may have temperature-dependent phase separation that couples to the membrane shape. At temperatures both (C) above and (D) below $T_{mix}$, an $L_d$ phase may sort to (E) the more curved regions in model membranes. This manifests as faster single-lipid diffusion correlated with the curved membrane with lipids diffusing faster in $L_d$ than $L_o$ phases. To see this figure in color, go online.

demonstrates how the plasma membrane may appear uniform in composition without large-scale phase separation yet utilize phase separation in the recruitment of membrane-bound molecules to or from endocytic pits.

## MATERIALS AND METHODS

This article incorporates a diverse collection of experimental and computational methods that are detailed in the supporting material. The formation of giant unilamellar vesicles (GUVs), SLBs, and nanoengineered substrates are detailed in supporting materials and methods S1 and S2. To maintain the large-scale phase separation in the SLBs like as observed on the GUVs, required precise temperature control of the sample and substrate was required during SLB formation (supporting materials and methods S3). The diffraction-limited imaging (supporting materials and methods S4) and single-molecule localizations (supporting materials and methods S5) occurred with precise sample temperature control (supporting materials and methods S6). Data analysis included spatial mapping of the lipid phases (supporting materials and methods S7), membrane curvature (supporting materials and methods S8), SPT (supporting materials and methods S9), and diffusion coefficient calculations (supporting materials and methods S10). Considerations of the effects of the fluorophore (supporting materials and methods S11) and the substrate (supporting materials and methods S12) on the lipid dynamics are presented. Computational approaches include the continuum simulations with explicit phase-curvature coupling (supporting materials and methods S13) and coarse-grained (CG) molecular dynamics simulations (supporting materials and methods S14).

## RESULTS

### Phase separation in planar SLBs

To assess the lipid phases within the membranes, we added fluorescence tracer lipids to ternary mixtures of DiPhyPC, DPPC, and cholesterol. Phase-separated GUVs were burst upon microscopy coverslips to create SLB patches with distinct lipid phases of similar size as present on the GUVs, i.e., >5-mm-wide domains. Bright domains on the membranes indicated the $L_d$ phase, dim domains indicated the $L_o$ phase, and black regions indicated the lack of an SLB over the coverslip (Fig. 2). Substrate-membrane interactions prevented the diffusion of domains in the SLB and the coalescence of optically resolvable lipid phases in SLBs that were created by small vesicle fusion. The fluorescence contrast between the $L_o$ and $L_d$ phases reflects the partition coefficient of the fluorescent lipid and the length of the tie line that separated the two phases. The $L_o$ and $L_d$ phases were more similar in brightness at higher choles-terol concentrations and at higher temperatures.

The observed $T_{mix}$ varies between SLB patches similar to the variation between GUVs in a sample (39). The $T_{mix}$ for planar SLBs with a molar ratio of 1:1:2

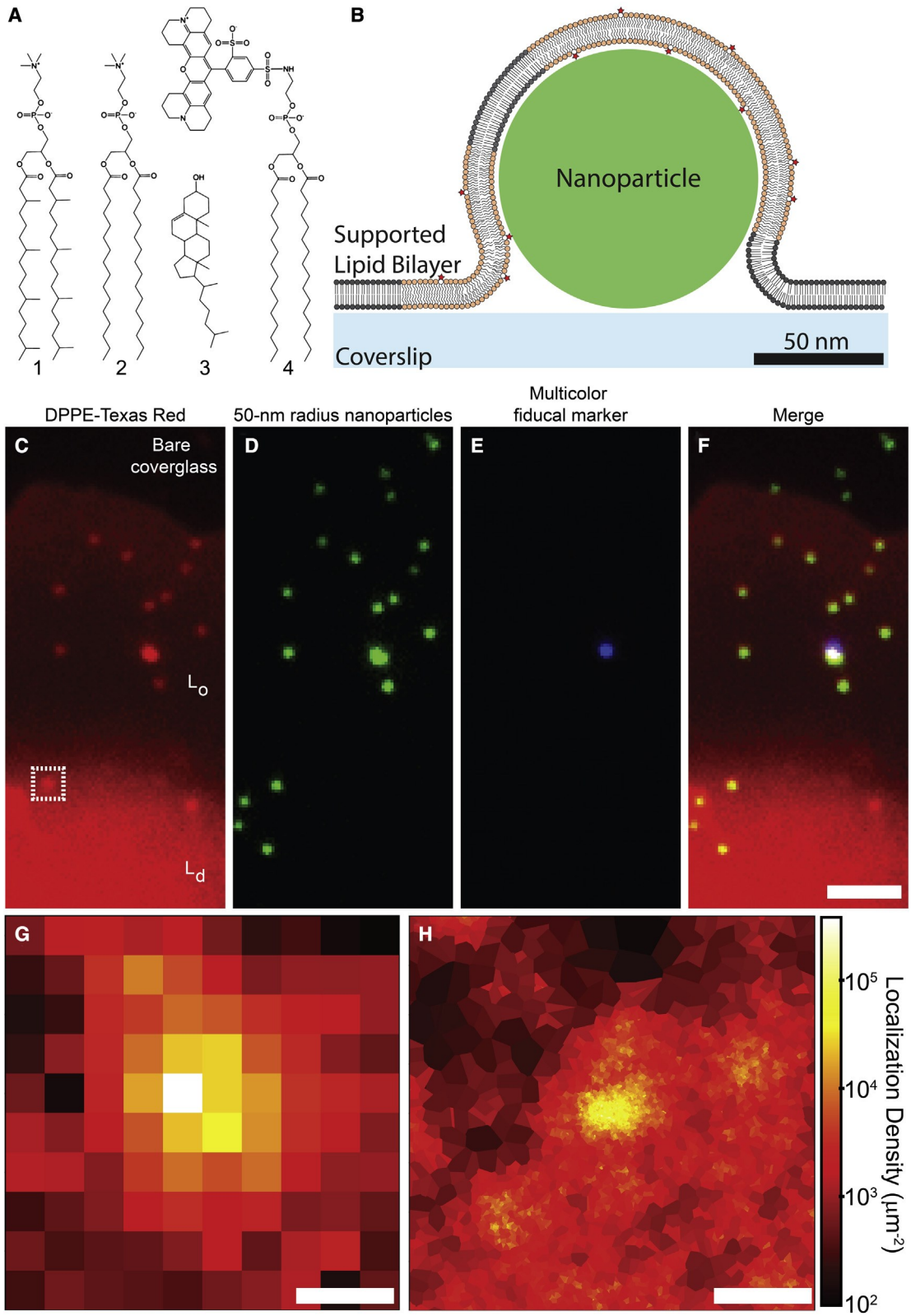


FIGURE 2 Phase-separated SLBs were created with nanoscale membrane curvature. (A) The lipids used include 1) DiPhyPC, 2) DPPC, 3) cholesterol, and 4) DPPE-Texas Red. (B) The lipid phases and single-lipid diffusion were experimentally measured relative to the engineered, nanoparticle-induced mem-brane curvature. (C–H) 1:1:2-M ratio of DiPhyPC:DPPC:cholesterol and 0.1 mol % DPPE-Texas Red is shown over 50-nm-radius nanoparticles. Multicol-ored, diffraction-limited fluorescence images include those of (C) DPPE-Texas Red, (D) the 100-nm diameter fluorescent nanoparticles, (E) the multicolored

(legend continued on next page)

DiPhyPC:DPPC:cholesterol was between 28C and 37C, as evident by the stable phase separation at 28C and the phase mixing at 37C (Fig. S1). The $T_{mix}$ for planar 2:2:1 SLBs was greater than 37C, as evident by the consistently sharp phase boundaries. All samples were equilibrated for >30 min prior to measuring the phase separation or lipid diffusion. The slow large-scale mixing of SLBs resulted in some of the largest domains (>10-mm diameter) remaining evident with blurred phase boundaries after equilibration at a temperature greater than $T_{mix}$, as described previously (34,40).

## $L_d$-preferring lipids sort to curvature

To measure if nanoscale membrane curvature preferentially recruited lipid phases, we engineered curvature in SLBs by bursting phase-separated GUVs over 50-nm-radius nanoparticles and glass coverslips (Fig. 2 B). Multicolor imaging provided tracking of the $L_d$-preferring tracer lipid density (Fig. 2 C); the fluorescent, 50-nm-radius, membrane-curvature-generating nanoparticles (Fig. 2 D); and the multicolor fiducial mark (Fig. 2 E) to ensure chromatic alignment and confirmation membrane bud locations. This setup provided a nanoengineered membrane shape while allowing individ-ual lipids to diffuse freely within the SLB. The connectivity of the membrane between the planar SLB and the membrane bud over the nanoparticle was demonstrated both with fluorescence recovery after photobleaching and the presence of uninterrupted single-lipid trajectories (Fig. S2) (26,41).

Lipid sorting was induced by membrane curvature with disorder-preferring fluorescent lipids concentrating on the curvature (Fig. 3). Quasi-single-component POPC and DiPhyPC membranes served as a control and normalization for the phase-independent increase in membrane area per pixel, brightness, and single-molecule sorting to curvature (Eq. S4). In all quasi-single-component membranes, no apparent sorting of the fluorescent lipids to the curvature was observed; the local increase in membrane brightness at the bud was consistent with an increase in membrane area projected onto the xy-imaging plane (37).

In mixed-composition membranes, the lipid phase on the curved membrane ($P_C$) was compared with the phase of the flat membrane ($P_F$) immediately surrounding each nanoparticle-supported membrane bud (Eqs. S3 and S4). $P_C$ and $P_F$ were measured for varying membrane compositions and temperatures. In SLBs with phase separation, lower temperatures provide a greater range in $P_F$ values, which is consistent with lower temperatures yielding longer tie lines and a wider variety in the fluorescent lipid density across the membrane (Fig. 3 A). The phase on membrane buds was highly correlated with the phase surrounding the bud (Fig. 3 B), but the phase on the bud was consistently more disordered than the surrounding phase (Fig. 3 C). The sorting of the $L_d$ phase to the curved membrane is evident by $P_C$ being greater than $P_F$, i.e., with the disorder-preferring probe localizing at curved regions. The ratio of $P_C/P_F$ is analogous to a curvature-dependent partition coefficient and a previously used quantification of phase sorting (15).

The $P_C/P_F$ ratio versus $P_F$ for different phase-separating lipid mixtures and temperatures show no clear change in $P_C/P_F$ ratio versus temperature. The $P_C/P_F$ ratio was greater than one for all temperatures and all values of $P_F$, which indicates that the curved membrane was consistently more concentrated in the disorder-preferring fluorescent lipid than the surrounding flat membrane (Fig. 3 C). Interestingly, the $P_C/P_F$ ratio was larger when $P_F$ was lower, which reveals that the curvature-induced sorting of lipid phases was strongest when the surrounding phase was more ordered. This is further shown by characterizing the lipid phase sorting for varying temperatures (Fig. 3 D). At all temperatures, the buds surrounded by the $L_o$ phase showed more curvature-induced sorting than the buds surrounded by the $L_d$ phase, and this is most clear at lower temperatures.

## Continuum simulations demonstrate curvature-induced lipid domains

To validate the experimental sorting results, we performed computational simulations of a curved membrane with a local phase governed by the continuum Landau theory and an explicit phase-curvature coupling constant (g) (Eq. S9). The membrane was modeled to have a topography consistent with the experimental, 50-nm-radius, nanoparticle-supported SLBs and divided into 3861 distinct cells each with an area of 9 $nm^2$ (Fig. S5). Landau phase constants and effective temperatures were chosen to provide two phases with realistic fluctuations in the local composition and phase boundaries, as described in the supporting material. Gaussian noise in the phase was added to each cell with each time step to model thermal fluctuations; a larger standard deviation (s) in this noise represented higher-temperature simulations.

At low temperature (s ¼ 0.07, T ¼ 15C), stable domains formed with fluctuations at the phase boundaries (Fig. 4 A). At a high temperature (s ¼ 0.08, T ¼ 35C), rapid fluctuations resulted in no large or stable phases present on the planar membrane (Fig. 4 B). The supporting material includes videos of these simulations and images of the average phase across the membrane during the simulation with varying temperature and phase–curvature coupling (Video S1; Fig. S6). The $L_d$ phase was sorted to the

nanoparticle fiducial markers, and (F) their merged image. (C) The phase-separated membrane contained a micron-scale $L_d$ domain (bright, bottom) and $L_o$ domain (dim, middle) while surrounded by bare coverslip (black, top). (G) Diffraction-limited and (H) super-resolution images of the membrane with engineered curvature revealed the sorting and diffusion of lipids from outlined region of (C). Scale bars represent (C–F) 2 mm or (G–H) 200 nm. To see this figure in color, go online.

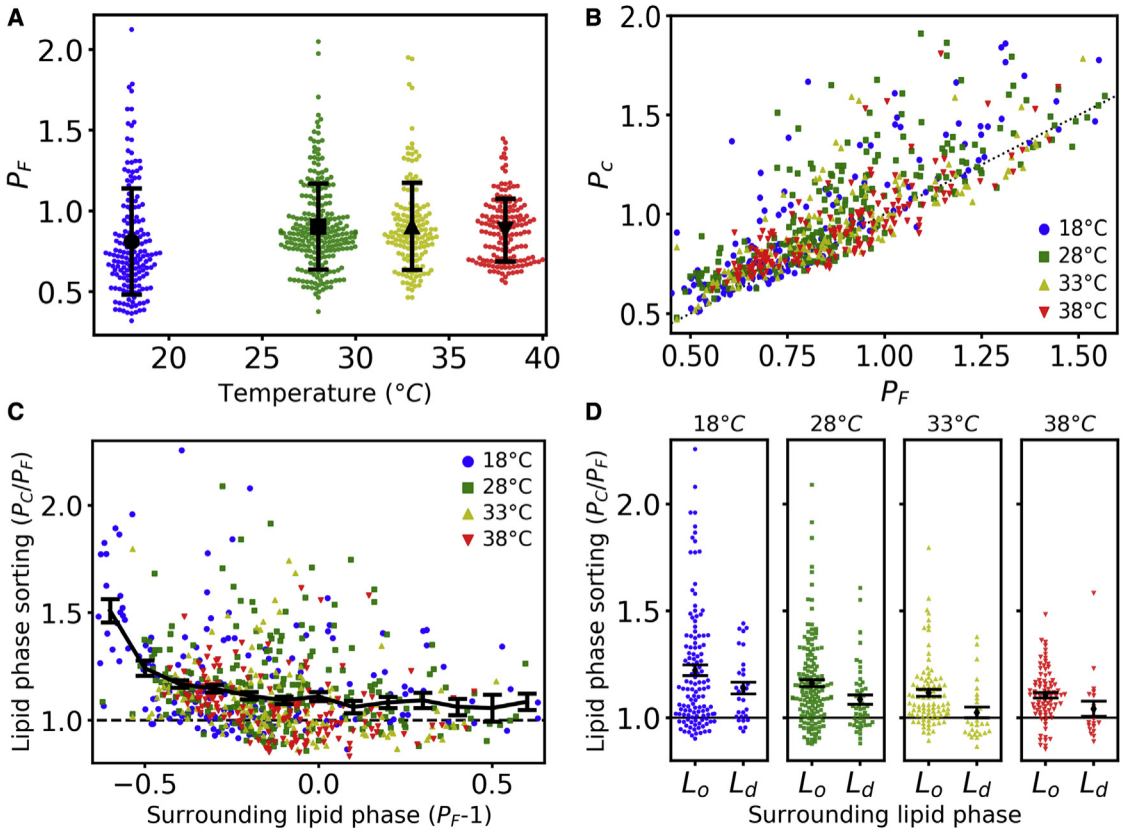


FIGURE 3 Curvature-induced phase sorting was observed in SLBs by assessing the phase on the curved and the surrounding flat membrane. Each data point here represents a single membrane bud in a membrane with an average 1:1:2-M ratio of DiPhyPC:DPPC:cholesterol. (A) A greater range of phases on the flat membrane ($P_F$) were observed at colder temperatures, consistent with colder temperatures providing longer tie lines; the black data represent the mean and the standard deviation of observations at each temperature. (B) The phase of the curved membrane ($P_C$) was more likely to be disordered if the surround-ing flat area was more disordered; the dotted line represents $P_C$ ¼ $P_F$ to guide the eye. (C) The normalized ratio of curved to flat phases reveals that greater phase sorting is observed when the surrounding membrane was more ordered, shown as larger $P_C/P_F$ ratio values when $P_F$ is smaller. Here, the black data represent the mean and standard error of $P_C/P_F$ for all temperatures as binned by P . (D) Grouping the data based on the $P_F$ <0.9 for $L_o$ and $P_F$ >1.1 for $L_d$ reveals that the $L_d$ phase sorted to the curvature at all temperatures; the black data represent the mean and standard error for each condition. To see this figure in color, go online.

curvature in a s- and g-dependent manner. At low temperatures, even weak phase-curvature coupling resulted in significant sorting of the $L_d$ phase to the membrane bud (Fig. 4 C). The phase sorting propagated onto the flat membrane surrounding the bud, which resulted in the planar membrane close to the curvature being more likely to be disordered than the planar membrane far from the curvature. The $L_d$ phase was also sorted to the curved membrane even at elevated temperatures when no large phases were observed on the planar membrane if g R0.1 (black arrow, Fig. 4 D).

This approach does not ensure consistent composition of the membrane during the simulation, i.e., the fraction of the membrane that is $L_d$ may change versus time. Further, this method does not reproduce phase fluctuation dynamics. This approach does allow for convergence of system to equilibrated membrane phase distribution. Accordingly, these simulations are used for revealing phase sorting relative to the curvature and not for diffusion of the lipids.

Because the phase-curvature coupling is explicitly included within Eq. S9, the sorting of the $L_d$ is expected. However, consequences of varying temperature and the propagation of the phase sorting to the surrounding planar membrane provided valuable cross-validation of the experimental and molecular dynamics results that were well represented by the applied Hamiltonian with only a first-order, linear phase-curvature coupling.

## Molecular dynamics simulations demonstrate spontaneous phase-curvature coupling

To further validate these results, CG molecular dynamics simulations were performed with nanoscale membrane curvature maintained by dummy particles (42). CG simulations provide single-molecule dynamics from a particular leaflet of the membrane of known shape without perturbations from fluorescent labels. CG simulations included a 5-nm-radius hemispherical bud connected to a planar

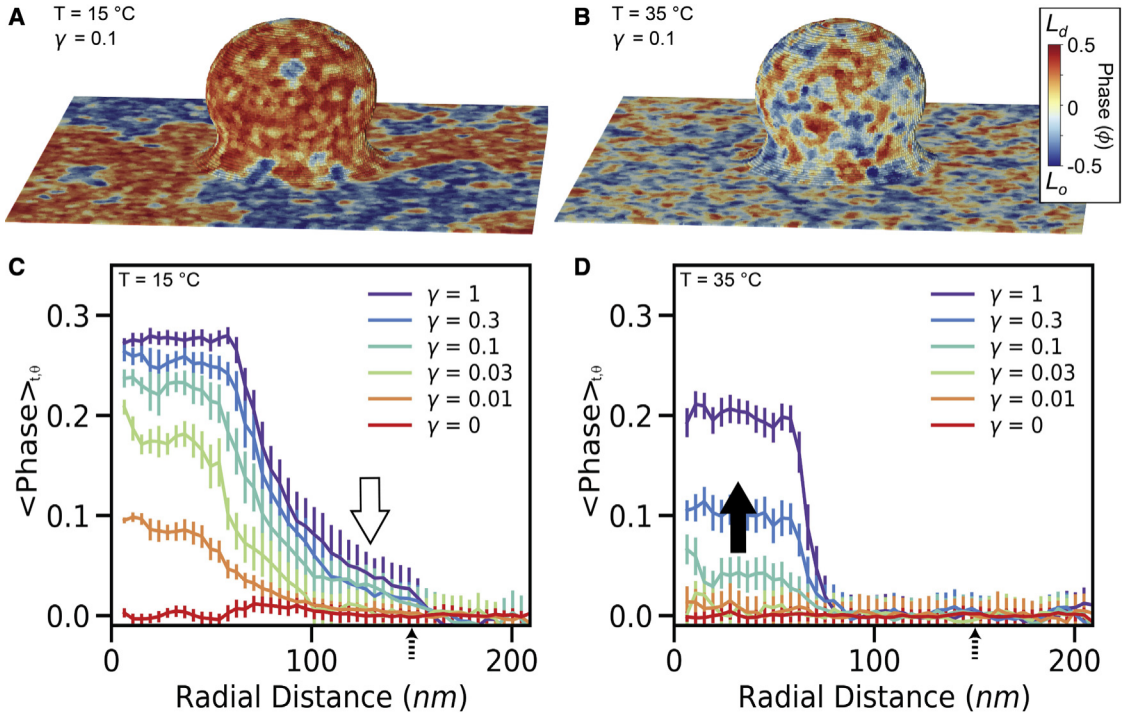


FIGURE 4 Continuum simulations that couple lipid phases to curvature were performed incorporating an explicit phase-curvature coupling (g). (A and B) Representative snapshots and (C and D) the time- (t) and azimuthally (q) averaged phase reveal the coupling between the temperature (T) and g. A Landau second-order phase transition was coupled with an effective temperature of (A and C) 15C or (B and D) 35C. (C) When bulk phase separation is stable, the curvature acts as a nucleation site with the $L_d$ phase concentrating at the curvature and propagating on to the surrounding planar membrane (white arrow). (D) When a higher temperature prevents bulk phase separation, a phase-curvature coupling may still induce the sorting of a disordered phase to the membrane bud (black arrow). The boundary of r R 1 5 0 nm (dashed arrow) was renormalized every frame to have equal $L_d$ and $L_o$ representation (i.e., < phase > r > 150 ¼ 0) to avoid the entire simulation from converging to a single phase. (C and D) The plotted data represents the mean and standard error of the equilibrated simulations. To see this figure in color, go online.

bilayer with a membrane neck of 5-nm minimum radius of curvature (Fig. 5; Video S2). The membranes had positive Gaussian curvature on the hemispherical bud top and negative curvature on the neck (Fig. S8 A). The simulated lipids diffused and sorted spontaneously relative with to the constant membrane shape according to the Martini force field (43).

The local concentrations of the individual lipid types were azimuthally averaged and displayed as 2D histograms (Fig. 5, C–F) or computed as the on-surface densities to show the relationship between membrane curvature and leaflet compositions (Fig. S8 B). Pure POPC bilayers, which are not capable of inducing a lipid phase separation, demonstrated no significant molecular-scale changes in lipid density with curvature (Fig. 5 F). However, for the commonly used phase-separating mixture of DPPC, DLiPC, and cholesterol, the membrane curvature recruited and concentrated the disorder-preferring DLiPC lipids while repelling the order-preferring DPPC and cholesterol. In both leaflets, DLiPC was concentrated on the hemispherical bud and the neck, consistent with experimental and continuum simulation results. The degree of phase separation of the individual leaflets was distinct, with the upper leaflet inducing a more pronounced sorting (Figs. 5 and S8), with a greater discussion of leaflet asymmetry being the focus of a future study.

## Single-lipid diffusion demonstrates the phase-curvature coupling

To test the effects of the phase-curvature coupling on lipid diffusion, experimental and computational SPT was performed to correlate the single-lipid dynamics with the membrane topography. The single-lipid trajectories were experimentally observed in SLBs with engineered membrane buds of 50-nm radius. The lipid phase, curvature, and temperature-dependent diffusion of DPPE-Texas Red was measured (Fig. 6). Diffusion was studied for SLBs of 1:0:0-, 1:1:2-, and 2:2:1-M ratios of DiPhyPC:DPPC:cholesterol. Each single-lipid step length through the xy plane was binned based on the radial lateral distance from the center of the membrane bud (r). Rayleigh distribution fitting of the single-step lengths in each bin provided a spatially mapped diffusion coefficient across the topographically varying SLB (37,41,44) (Eq. S5). This SPT analysis method provides greater spatial resolution of lipid diffusion than the conventional fluorescence recovery after photobleaching or mean-squared displacement versus

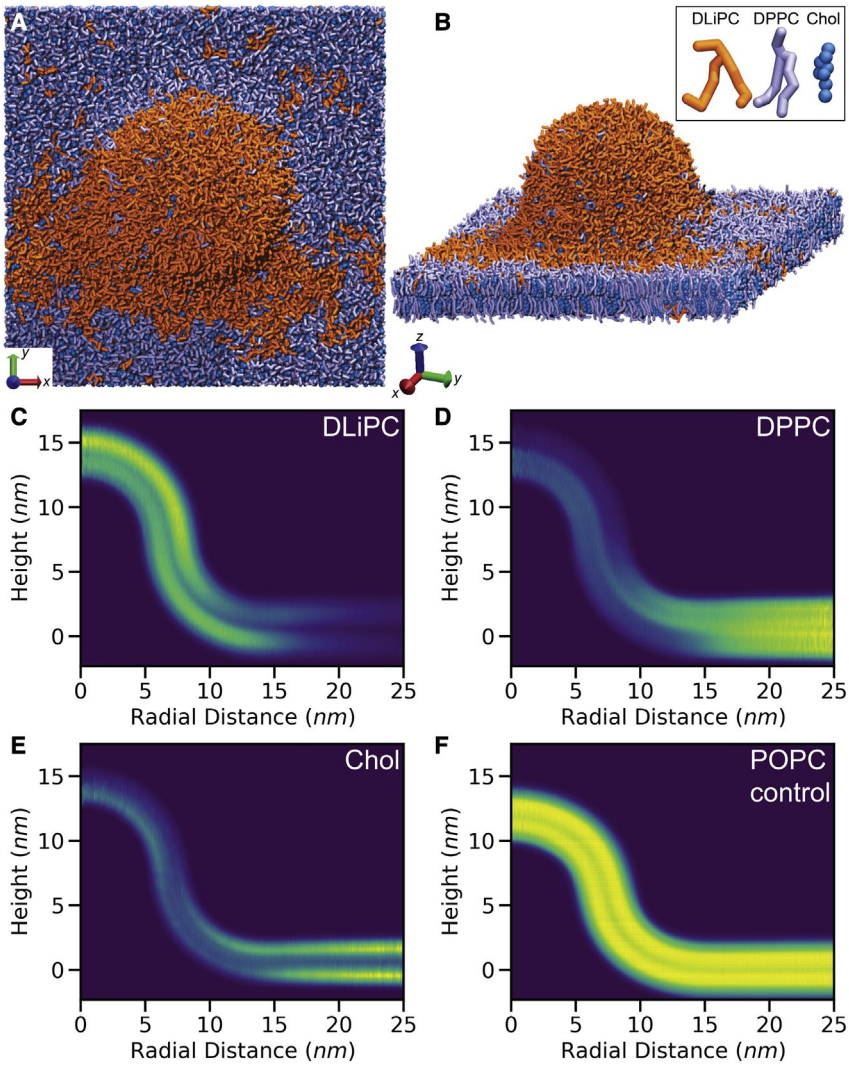


FIGURE 5 Coarse-grained molecular dynamics simulations spontaneously demonstrated phase-curvature coupling through lipid sorting and diffusion. (A and B) Coarse-grained simulations of a mixture of DLiPC, DPPC, and cholesterol revealed the coupling of phase separation to membrane curvature. Normalized 2D histograms show the azimuthally averaged density of lipid beads for each lipid type with (C) the $L_d$-preferring DLiPC concentrating on the bud with the $L_o$-preferring (D) DPPC and (E) cholesterol concentrating on the flat membrane. (F) POPC-only simulations reveal near uniform lipid densities throughout the simulation. To see this figure in color, go online.

lag time (Dt) analysis (45). Fluorescence recovery after photobleaching typically reports the mean diffusion over a diffraction-limited region of interest, and mean-squared displacement versus Dt typically averages together the diffusers' entire >1-mm trajectories (Fig. S7) (45).

The radially dependent diffusion through the xy plane ($D_{xy}$) varied with membrane topography due to both the curvature-dependent lipid mobility and the geometrical effects of projecting the 3D lipid trajectories into the imaging plane. Without correction, the $D_{xy}$ is smaller on the membrane bud because the lipid diffuses significantly in the Z-direction, which is not detected. It is critical to remove this geometrical consideration from the observed $D_{xy}$ prior to analyzing the diffusion on the curved versus flat membrane. The contribution due to projecting the curved membrane on to the xy-imaging plane was estimated from Monte Carlo simulations and subtracted to reveal an effective diffusion rate of the lipids on the curved ($D_C$) and flat membrane ($D_F$), as described in the supporting material (Eqs. S7 and S8). As the temperature increased, $D_F$ increased, as expected (37,46–48), showing that hotter membranes display faster diffusion.

To measure the phase- and curvature-dependent lipid diffusion, membrane buds were grouped based on the membrane composition, temperature, and surrounding phase. The individual curvature events were deemed $L_d$ or $L_o$ phase if $P_F$ was greater than 1.1 or less than 0.9, respectively. The curvature-dependent effects on diffusion were calculated through the projection-corrected ratios of $D_C/D_F$. All values of the $D_C/D_F$ ratios for ternary mixtures were greater than or equal to one; the lipids in phase-separated membranes diffuse faster if the membrane is curved (Fig. 6 D). The greatest $D_C/D_F$ ratio was observed in 20C SLBs with a 2:2:1-M ratio of DiPhyPC:DPPC:cholesterol when the buds were surrounded by $L_o$ phase when $D_C/D_F$ ¼ 2.3 5 1. The $D_C/D_F$ ratios were larger at colder temperatures, consistent with the $L_d$-preferring lipids sorting to the curvature more when the tie line separating the phases was longer, as also seen in the continuum models (Fig. 4).

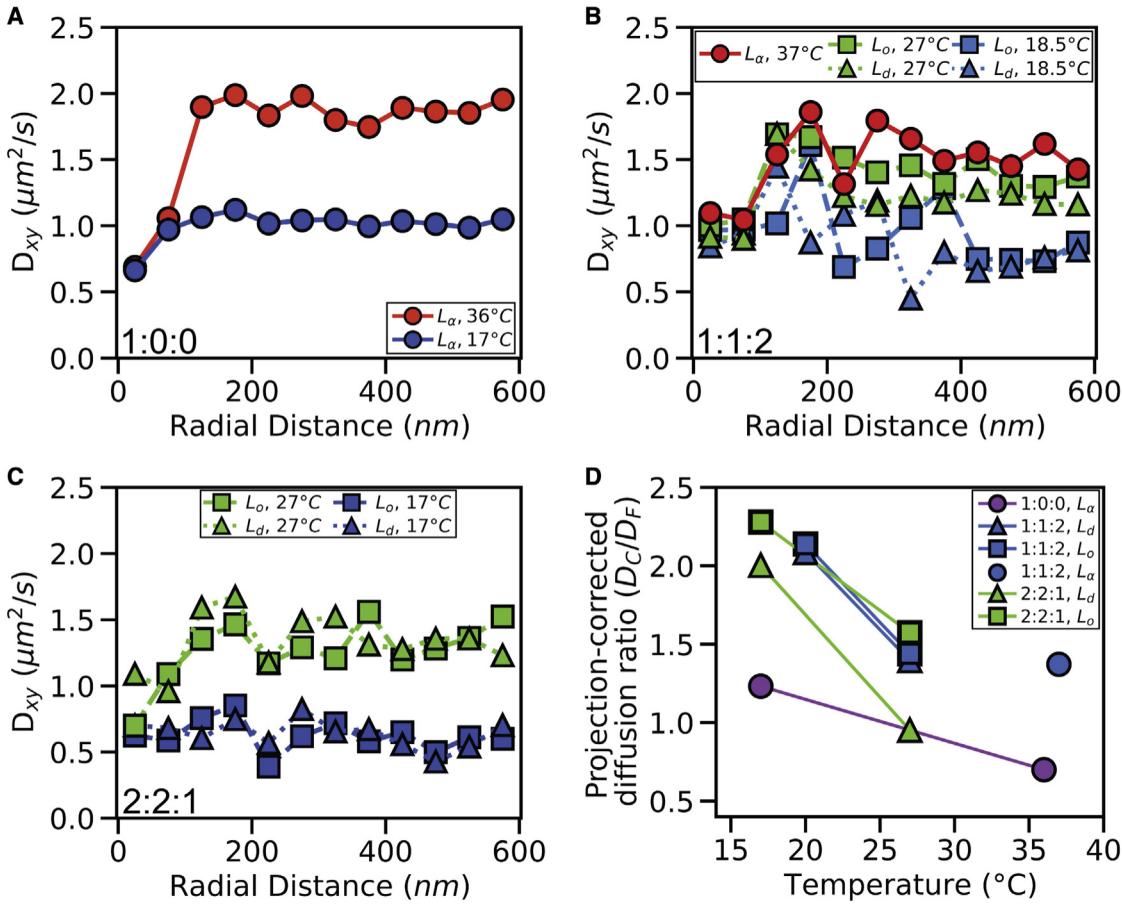


FIGURE 6 Curvature and phase separation influence lipid mobility. The lipid diffusion rate as projected into the xy plane ($D_{xy}$) was measured versus the radial distance away from the center of the membrane buds for (A) DiPhyPC membrane and phase-separated membranes composed of (B) 1:1:2- or (C) 2:2:1-M ratio of DiPhyPC:DPPC:cholesterol. Monte Carlo fitting to the diffusion through the xy plane yielded the in-membrane diffusion rate to extract the local in-membrane diffusion rates by correcting for the effects of projecting the 3D membrane shape into the xy-imaging plane. (D) The ratio of the in-membrane diffusion rates on the curved versus flat membranes ($D_C/D_F$) are shown for varying membrane compositions, phases, and temperatures. Uncertainty levels for each data point are given in Table S1. To see this figure in color, go online.

Interestingly, $D_{xy}$ decreased as r increased from 125 to 400 nm in ternary mixtures with clear phase separation (i.e., at lower temperatures and higher cholesterol content) (Fig. 6 B). The noise in the data made this trend subtle, but the $D_{xy}$ values for r ¼ 150–200 nm were consistently higher than the data points for r ¼ 350–400 nm. This trend is most obvious for the 1:1:2 composition at 18.5C data.

This decreasing $D_{xy}$ on the flat membrane near the curvature may be due to curvature-seeded $L_d$ phase propagation onto the planar SLB surrounding the nanoparticle, as was also seen in both the continuum and CG computational simulations (Figs. 4C, 5C, and 7B).

The CG simulations were also analyzed with single-lipid tracking analogously to how the experimental data was analyzed. CG simulations enable analysis with submicrosecond Dt and with no localization imprecision ($s_r$). When analyzed with Dt ¼ 100 ns, the POPC lipids displayed minimal difference in diffusion on the hemispherical bud versus the planar bilayer (i.e., r < 3 versus r > 13 nm), which shows that diffusion rates are unchanged by curvature in the absence of phase separation (Fig. 7 A). The lower $D_{xy}$ for the POPC lipids at r ¼ 8 nm is attributed to the effects of projecting the 3D lipid locations into the xy plane, while motion along the z axis was not incorporated. However, upon the incorporation of phase-separated lipid mixtures, all lipid types experienced faster diffusion on the membrane bud with Dt ¼ 100 ns, correlated with the curvature-sorted $L_d$ phase. The curvature-associated $L_d$ phase provided a lower effective membrane viscosity such that all lipids in the phase-separated membrane diffused faster on the bud.

Analysis of the CG simulations was also performed with conditions mimicking those achieved experimentally (Fig. 7 B). These computationally feasible, 5-nm-bud CG simulations were analyzed with larger $s_r$ and Dt values so that similar spatial and temporal blurring was incorporated into both the CG and experimental data. To make the 5-nm CG buds mimic the 50-nm experimental buds, the CG lipid locations were blurred with $s_r$ applied at 10% of the experimental conditions (2 and 20 nm, respectively). The Dt used for the mimicking CG analysis was 0.1% of that used experimentally (2 ms and 2 ms,

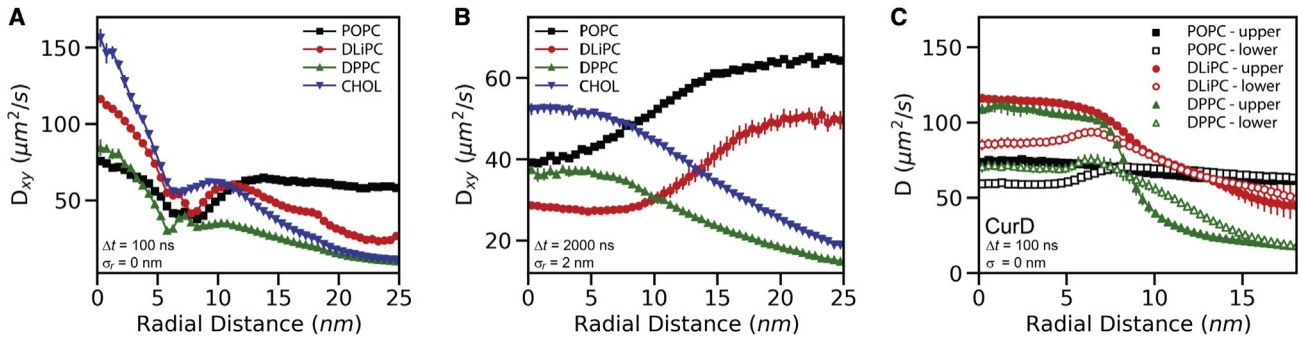


FIGURE 7 The single-lipid step lengths from coarse-grained molecular dynamics simulations were analyzed to mimic the experimental analysis condi-tions for phase-separated and pure POPC compositions by calculating the diffusion rate through the XY plane ($D_{xy}$). Compared with the experimental ca-pabilities, molecular dynamics simulations provided a more frequent observation and greater certainty of the lipid locations over a smaller membrane bud. (A) When mean-squared displacement analysis included Dt ¼ 100 ns and no artificially added localization uncertainty (sr ¼ 0), diffusion was faster on the curved membrane for all lipid types, consistent with the $L_d$ phase sorting to the curvature. (B) But with analysis conditions that mimic the experimental conditions and incorporate greater spatial averaging (Dt ¼ 2 ms; sr ¼ 2 nm), then $D_{xy}$ showed lipid-type dependencies. Here, the $L_d$-partitioning DLiPC and POPC show great qualitative diffusion similarities to the $L_d$-partitioning DPPE-TR observed experimentally (Fig. 6). (C) Molecular dynamics results were additionally subjected to a diffusion analysis with geodesic distance-based algorithms (CurD) to reveal the in-membrane diffusion separate from any pro-jection effects. Here, the consistent curvature of the membrane bud had uniform diffusion rate without projection effects. Plotted data represents the mean and standard error of the equilibrated simulations. To see this figure in color, go online.

respectively) to account for the quadratic dependence of the lag time with the expected step length and the 10faster diffu-sion observed in CG simulations versus experimental mea-surements (49). These analysis conditions resulted in consistent ratios of the localization uncertainty and mean step length to the curvature radius for both the CG simulations and experimental conditions. Additionally, the $D_{xy}$ results pre-sented from CG simulations were corrected with Eq. S6, as done experimentally.

When analyzing the POPC diffusion with longer time steps (Dt ¼ 2 ms) and incorporating a localization uncer-tainty ($s_r$ ¼ 2 nm) to mimic the spatial blurring observed experimentally, $D_{xy}$ versus r for CG POPC closely resem-bles experimental results for nanoscale buds in quasi-sin-gle-component SLBs (Figs. 6 A and 7 B) with the changes in $D_{xy}$ dominated by geometrical projection effects (Fig. 7 C) (37,45). With Dt ¼ 2 ms and $s_r$ ¼ 2 nm, the diffusion of CG DLiPC resembles that of the CG POPC and experi-mental DPPE-Texas Red results, but the DPPC and choles-terol diffusion shows a significant increase in $D_{xy}$ on the bud versus the surrounding planar membrane. This result further supports the observation of curvature-phase coupling and motivates the incorporation of an order-preferring fluores-cent lipid in future experimental studies.

CG simulations provide the full 3D trajectory of each lipid, which enables resolving leaflet differences and removing the influence projecting lipids onto an imaging plane via the use of a geodesic distance-based analysis of the CG simulations (50). While the nuances of lipid diffusivity in spatially varying mean and Gaussian curvature are the focus of an upcoming article, here we present the key results of the geodesic dis-tance-based analysis, named CurD. To gain insight into the detailed lipid dynamics, the averaging effect of measurement time was mitigated by extracting the diffusion coefficients for displacements Dt ¼ 1 (Fig. S8 C) and 100 ns (Fig. 7 C). Both leaflets provided faster diffusion on the bud for phase-sepa-rated membranes. However, the use of geodesic distances demonstrated that the experimentally apparent slowing of lipids at 7 nm from the bud center is indeed due to the 2D pro-jection of the 3D trajectories rather than a reflection of effec-tive local membrane viscosity changes. Furthermore, it was revealed that the observed increase in lipid mobility correlated with the mean curvature. For a given lipid type, diffusion rates in the planar membrane region converged to a single value across both leaflets. Hydrodynamics dictates that the effective viscosity in a single phase should be the same for all lipid types (51). Here, the ratio of diffusion for DLiPC and DPPC lipids was closer to 0.5, which matched the ratio of diffusion coeffi-cients in Martini simulations of planar phase-separating sys-tems (52). This finding agrees with the observation that the lipid phases propagated along the flat membrane and spanned the simulation box.

## DISCUSSION

This study provides a quantitative analysis of the phase-curva-ture coupling in membranes with shapes that are reminiscent of nanoscopic endocytic pits and viral buds. The membrane composition, temperature, and curvature were varied for experimental and simulated membranes. The phase-curvature coupling was revealed by the lateral heterogeneity in both the local density and the diffusion rates of disorder-preferring lipids by both experimental and computational methods. The curvature influenced the lipids more under conditions that provided a longer tie line separating the coexisting phases, i.e., lower temperature and less cholesterol. This may be ex-plained by the correlation that the more ordered the surround-ing phase, the higher its bending modulus. Thus, in mixtures

where the ordered phase has a low concentration of DiPhyPC, the energetic penalty for placing the ordered phase in the curved regions is high, leading to a more significant curvature-regulated sorting of the lipid phases.

The effects of curvature were still present in lipid mixtures when no phase separation was observed on the planar membrane, which suggests that the curvature was able to induce a phase separation and demonstrates the strength of our techniques to reveal nanoscopic lipid phases. This is consistent with a curvature-induced phase separation and that $T_{mix}$ is dependent on the membrane shape. While pushing the limits of experimental and computational feasibility, these diverse methods provided broad agreement to provide cross-validation between the four complementary approaches employed. These results suggest that the dynamic curvature and composition of native biological membranes may couple to drive complex membrane processes in membrane signaling, shape changes, and pathophysiology.

## Membrane brightness at curvature sites

The 1:1:2 SLB phase sorting result indicated that the experimental ratio of $P_C/P_F$ was greater than one for all values of $P_F$ (Figs. 3 and S4); the disorder-preferring fluorescent lipid density was higher on curved membranes. The sorting was presumably due to the differences in the phase bending rigidity because the leaflets seemed to maintain phase registration, and we do not anticipate that the molecular shape (e.g., the lipid packing parameter) of the fluorescent lipid was sufficient to induce significant single-molecule, phase-independent sorting (18,25,53). This is further supported by our observation that quasi-one-component membranes of POPC were not able to induce a curvature-dependent sorting of fluorescent lipids experimentally or alter the POPC density in CG simulations (Fig. 5 F) (37).

## Diffusion reveals the coupling of phases and curvature

The ratio of diffusion on curved versus flat membranes ($D_C/D_F$) was larger when phase separation was present (Fig. 6). Quasi-one component $L_d$ membranes of DiPhyPC displayed no significant difference between $D_C$ and $D_F$, whereas mixtures of DiPhyPC, DPPC, and cholesterol displayed faster diffusion at curved surfaces regardless of if phase separation was observed on the planar membrane. This result is consistent with sorting studies where $P_C/P_F$ values were above one for all $P_F$ (Fig. 3 C) and the CG simulations (Figs. 7 and S8). We hypothesize that this demonstrates the capability of curvature to induce phase separation that was not present on flat membranes by effectively increasing the local $T_{mix}$.

We did not observe a difference in the diffusion ratio $D_C/D_F$ for membranes of varying surrounding phases, which was likely due to the intrinsic noise in the determination of the membrane phase surrounding each membrane bud. These diffusion studies were practically limited in the number of membrane buds able to be measured, the uncertainty of the phase at 400-nm away from each bud, and the single-lipid diffusion rates measured at each radial distance.

## Curvature-seeded phase separation propagates onto the surrounding flat membrane

A subtle but consistent decrease in $D_{xy}$ was observed on the flat membrane propagating away from the engineered curvature sites (Fig. 6 B). This demonstrates that the effective membrane viscosity and the composition of the flat membrane varied with distance from the nanoparticle as if the curvature seeded a phase separation that propagated onto the surrounding flat membrane. This phenomenon was also observed in continuum and CG simulations of phase separation, with the $L_d$ phase more likely to be present on the flat membrane that is near the curvature versus far from the curvature. (Figs. 4 and 5). This seeding effect may prove to provide a longer-rate attraction of membrane components to the curvature sites. If the curvature sites can seed a phase separation and an extended gradient of the curvature-preferring phase onto the surrounding planar membrane, then the curvature site may more affectively recruit membrane-bound molecules into the membrane bud for selective endocytosis and trafficking.

## Conclusions

Nanoscale membrane curvature was engineered in phase-separated SLBs. The sorting and dynamics of lipids were measured to reveal the curvature-induced phase separation and the phase-curvature coupling at physiological length scales. The fluorescence intensity ratio of curvature versus surrounding planar bilayer from diffraction-limited images show the $L_d$-preferring lipids sorted to the engineered curvature. The single-lipid diffusion rates were measured versus the lateral distance away from the center of curvature to further support the curvature-induced sorting of disordered lipids. Unlike quasi-one-component liquid DiPhyPC or POPC bilayers, SLBs with ternary mixtures of lipids showed a faster diffusion on the curved versus flat membranes. The effects of curvature on lipid diffusion and sorting were more pronounced under conditions in which the phase-separating tie lines were longer, including lower temperatures and less cholesterol, and when the local surrounding planar membrane was more ordered. These results indicate that the strong preference of disorder-preferring lipids to membranes curved at physiological scales.

These results demonstrate that the interplay between lipid phases and membrane shape may contribute to the cellular needs for lateral sorting on the membrane. Whereas single-molecule sorting to membrane buds may be too weak for a significant change in the membrane composition due to the curvature, the collective behavior of the lipids through

phase separation may induce substantial changes to the membrane composition and behavior. For example, the sorting of lipid phases relative to membrane curvature would both induce changes to the local membrane protein composition and affect further membrane shape changes, such as by altering the local membrane bending stiffness and leaflet asymmetry. In symmetric model membranes, the $L_d$ phase is concentrated on more curved membranes due to the lower bending stiffness of the $L_d$ phase relative to the $L_o$ phase, but live cell membranes frequently have membrane buds correlated with $L_o$ phases. This difference may come from the leaflet asymmetry in live cells, which induces a phase-dependent intrinsic curvature, i.e., the $L_o$ phase may have an energy minimum in a curved geometry, while the $L_d$ phase may prefer to be planar. The interplay between lipid phase and membrane shape is potentially of fundamental importance for essential plasma membrane and organelle functions. The experimental and computational results presented here reveal ability and limitations of <100-nm membrane buds to induce and sort lipid phases.

## SUPPORTING MATERIAL

Supporting material can be found online at https://doi.org/10.1016/j.bpj.2023.01.001.

## AUTHOR CONTRIBUTIONS

X.W., M.J., B.F., and C.V.K. wrote the manuscript. X.W. and C.V.K. designed the experiments and performed the data analysis. X.W. performed the experiments. C.V.K. performed the continuum simulations. M.J. and B.F. performed the CG simulations.

## ACKNOWLEDGMENTS

The authors thank Aurelia R. Honerkamp-Smith for valuable discussions. CSC-IT Center of Science is acknowledged for computational resources. X.W. was supported by the Thomas C. Rumble University graduate fellowship, Wayne State University Summer Dissertation Award, and the Richard Barber Interdisciplinary Research Program. M.J. was supported by an Academy of Finland postdoctoral researcher grant (grant no. 338160) and the Emil Aaltonen Foundation. This material is based upon work supported by the National Science Foundation under grant no. DMR1652316.

## DECLARATION OF INTERESTS

The authors declare no competing interest.

## SUPPORTING CITATIONS

The following reference appears in the Supplemental Information: (54–69).

## REFERENCES

1. Pralle, A., P. Keller, . , J. K. Hörber. 2000. Sphingolipid–cholesterol rafts diffuse as small entities in the plasma membrane of mammalian cells. J. Cell Biol. 148:997–1008.
2. Simons, K., and E. Ikonen. 1997. Functional rafts in cell membranes. Nature. 387:569–572.
3. Honerkamp-Smith, A. R., P. Cicuta, . , S. L. Keller. 2008. Line tensions, correlation lengths, and critical exponents in lipid membranes near critical points. Biophys. J. 95:236–246.
4. Shaw, T. R., S. Ghosh, and S. L. Veatch. 2021. Critical phenomena in plasma membrane organization and function. Annu. Rev. Phys. Chem. 72:51–72.
5. Fessler, M. B., and J. S. Parks. 2011. Intracellular lipid flux and membrane microdomains as organizing principles in inflammatory cell signaling. J. Immunol. 187:1529–1535.
6. Hurley, J. H., E. Boura, . , B. Różycki. 2010. Membrane budding. Cell. 143:875–887.
7. Simons, K., and D. Toomre. 2000. Lipid rafts and signal transduction. Nat. Rev. Mol. Cell Biol. 1:31–39.
8. Waheed, A. A., and E. O. Freed. 2010. The role of lipids in retrovirus replication. Viruses. 2:1146–1180.
9. Mukherjee, S., and F. R. Maxfield. 2000. Role of membrane organization and membrane domains in endocytic lipid trafficking. Traffic. 1:203–211.
10. Parton, R. G., and K. Simons. 2007. The multiple faces of caveolae. Nat. Rev. Mol. Cell Biol. 8:185–194.
11. Parton, R. G., M. A. Del Pozo, . , C. Lamaze. 2020. Caveolae: the FAQs. Traffic. 21:181–185.
12. Veatch, S. L., and S. L. Keller. 2002. Organization in lipid membranes containing cholesterol. Phys. Rev. Lett. 89:268101.
13. Veatch, S. L., and S. L. Keller. 2005. Seeing spots: complex phase behavior in simple membranes. Biochim. Biophys. Acta. 1746:172–185.
14. Roux, A., D. Cuvelier, . , B. Goud. 2005. Role of curvature and phase transition in lipid sorting and fission of membrane tubules. EMBO J. 24:1537–1545.
15. Sorre, B., A. Callan-Jones, . , P. Bassereau. 2009. Curvature-driven lipid sorting needs proximity to a demixing point and is aided by proteins. Proc. Natl. Acad. Sci. USA. 106:5622–5626.
16. Tian, A., and T. Baumgart. 2009. Sorting of lipids and proteins in membrane curvature gradients. Biophys. J. 96:2676–2688.
17. Heinrich, M., A. Tian, . , T. Baumgart. 2010. Dynamic sorting of lipids and proteins in membrane tubes with a moving phase boundary. Proc. Natl. Acad. Sci. USA. 107:7208–7213.
18. Kamal, M. M., D. Mills, . , J. Howard. 2009. Measurement of the membrane curvature preference of phospholipids reveals only weak coupling between lipid shape and leaflet curvature. Proc. Natl. Acad. Sci. USA. 106:22245–22250.
19. Ogunyankin, M. O., D. L. Huber, . , M. L. Longo. 2013. Nanoscale patterning of membrane-bound proteins formed through curvature-induced partitioning of phase-specific receptor lipids. Langmuir. 29:6109–6115.
20. Yoon, T.-Y., C. Jeong, . , S.-D. Lee. 2006. Topographic control of lipid-raft reconstitution in model membranes. Nat. Mater. 5:281–285.
21. Parthasarathy, R., C. h. Yu, and J. T. Groves. 2006. Curvature-modulated phase separation in lipid bilayer membranes. Langmuir. 22:5095–5099.
22. Baumgart, T., S. Das, . , J. T. Jenkins. 2005. Membrane elasticity in giant vesicles with fluid phase coexistence. Biophys. J. 89:1067–1080.
23. Waheed, A. A., and E. O. Freed. 2009. Lipids and membrane microdomains in HIV-1 replication. Virus Res. 143:162–176.
24. Lipowsky, R. 1993. Domain-induced budding of fluid membranes. Biophys. J. 64:1133–1138.
25. Cooke, I. R., and M. Deserno. 2006. Coupling between lipid shape and membrane curvature. Biophys. J. 91:487–495.
26. Cheney, P. P., A. W. Weisgerber, . , M. K. Knowles. 2017. Single lipid molecule dynamics on supported lipid bilayers with membrane curvature. Membranes. 7:15.

27. Larsen, J. B., M. B. Jensen, . , D. Stamou. 2015. Membrane curvature enables N-Ras lipid anchor sorting to liquid-ordered membrane phases. Nat. Chem. Biol. 11:192–194.
28. Dietrich, C., L. A. Bagatolli, . , E. Gratton. 2001. Lipid rafts reconstituted in model membranes. Biophys. J. 80:1417–1428.
29. Scherfeld, D., N. Kahya, and P. Schwille. 2003. Lipid dynamics and domain formation in model membranes composed of ternary mixtures of unsaturated and saturated phosphatidylcholines and cholesterol. Biophys. J. 85:3758–3768.
30. Filippov, A., G. Orädd, and G. Lindblom. 2004. Lipid lateral diffusion in ordered and disordered phases in raft mixtures. Biophys. J. 86:891–896.
31. Chiantia, S., J. Ries, . , P. Schwille. 2006. Combined AFM and two-focus SFCS study of raft-exhibiting model membranes. ChemPhysChem. 7:2409–2418.
32. Ge, Y., J. Gao, . , C. A. Naumann. 2018. Changes in cholesterol level alter integrin sequestration in raft-mimicking lipid mixtures. Biophys. J. 114:158–167.
33. Wu, H.-M., Y.-H. Lin, . , C.-L. Hsieh. 2016. Nanoscopic substructures of raft-mimetic liquid-ordered membrane domains revealed by high-speed single-particle tracking. Sci. Rep. 6:20542.
34. Woodward, X., and C. V. Kelly. 2020. Single-lipid dynamics in phase-separated supported lipid bilayers. Chem. Phys. Lipids. 233:104991.
35. Gov, N. S. 2006. Diffusion in curved fluid membranes. Phys. Rev. E Stat. Nonlin. Soft Matter Phys. 73:041918.
36. Domanov, Y. A., S. Aimon, ., P. Bassereau. 2011. Mobility in geometrically confined membranes. Proc. Natl. Acad. Sci. USA. 108:12605–12610.
37. Woodward, X., E. E. Stimpson, and C. V. Kelly. 2018. Single-lipid tracking on nanoscale membrane buds: the effects of curvature on lipid diffusion and sorting. Biochim. Biophys. Acta. Biomembr. 1860:2064–2075.
38. Yesylevskyy, S. O., T. Rivel, and C. Ramseyer. 2017. The influence of curvature on the properties of the plasma membrane. Insights from atomistic molecular dynamics simulations. Sci. Rep. 7:16078.
39. Veatch, S. L., and S. L. Keller. 2003. A closer look at the canonical 'raft mixture' in model membrane studies. Biophys. J. 84:725–726.
40. Gunderson, R. S., and A. R. Honerkamp-Smith. 2018. Liquid-liquid phase transition temperatures increase when lipid bilayers are supported on glass. Biochim. Biophys. Acta. Biomembr. 1860:1965–1971.
41. Kabbani, A. M., and C. V. Kelly. 2017. The detection of nanoscale membrane bending with polarized localization microscopy. Biophys. J. 113:1782–1794.
42. Boyd, K. J., and E. R. May. 2018. BUMPy: a model-independent tool for constructing lipid bilayers of varying curvature and composition. J. Chem. Theory Comput. 14:6642–6652.
43. Marrink, S. J., H. J. Risselada, . , A. H. de Vries. 2007. The MARTINI force field: coarse grained model for biomolecular simulations. J. Phys. Chem. B. 111:7812–7824.
44. Kabbani, A. M., K. Raghunathan, . , C. V. Kelly. 2020. Structured clustering of the glycosphingolipid GM1 is required for membrane curvature induced by cholera toxin. Proc. Natl. Acad. Sci. USA. 117:14978–14986.
45. Kabbani, A. M., X. Woodward, and C. V. Kelly. 2017. Revealing the effects of nanoscale membrane curvature on lipid mobility. Membranes. 7:60.
46. Bag, N., D. H. X. Yap, and T. Wohland. 2014. Temperature dependence of diffusion in model and live cell membranes characterized by imaging fluorescence correlation spectroscopy. Biochim. Biophys. Acta. 1838:802–813.
47. Sengupta, P., A. Hammond, . , B. Baird. 2008. Structural determinants for partitioning of lipids and proteins between coexisting fluid phases in giant plasma membrane vesicles. Biochim. Biophys. Acta. 1778:20–32.
48. Tamm, L. K. 1988. Lateral diffusion and fluorescence microscope studies on a monoclonal antibody specifically bound to supported phospholipid bilayers. Biochemistry. 27:1450–1457.
49. Marrink, S. J., and D. P. Tieleman. 2013. Perspective on the Martini model. Chem. Soc. Rev. 42:6801–6822.
50. Fábián, B., and M. Javanainen. 2021. CurD: a tool for diffusion analyses on curved membranes. Preprint at ChemRxiv. https://chemrxiv.org/engage/chemrxiv/article-details/6162d1ad8b620d83564a965d.
51. Lindblom, G., G. Orädd, and A. Filippov. 2006. Lipid lateral diffusion in bilayers with phosphatidylcholine, sphingomyelin and cholesterol: an NMR study of dynamics and lateral phase separation. Chem. Phys. Lipids. 141:179–184.
52. Thallmair, S., M. Javanainen, . , S. J. Marrink. 2021. Nonconverged constraints cause artificial temperature gradients in lipid bilayer simulations. J. Phys. Chem. B. 125:9537–9546.
53. Callan-Jones, A., B. Sorre, and P. Bassereau. 2011. Curvature-Driven lipid sorting in biomembranes. Cold Spring Harb. Perspect. Biol. 3:a004648.
54. Jaqaman, K., D. Loerke, . , G. Danuser. 2008. Robust single-particle tracking in live-cell time-lapse sequences. Nat. Methods. 5:695–702.
55. Kabbani, A. M., and C. V. Kelly. 2017. Nanoscale membrane budding induced by CTxB and detected via polarized localization microscopy. Biophys. J. 113:1795–1806.
56. Ovesný, M., P. Krízek, . , G. M. Hagen. 2014. ThunderSTORM: a comprehensive ImageJ plug-in for PALM and STORM data analysis and super-resolution imaging. Bioinformatics. 30:2389–2390.
57. Lagerholm, B. C., D. M. Andrade, . , C. Eggeling. 2017. Convergence of lateral dynamic measurements in the plasma membrane of live cells from single particle tracking and STED-FCS. J. Phys. D Appl. Phys. 50:063001.
58. Qian, H., M. P. Sheetz, and E. L. Elson. 1991. Single particle tracking. Analysis of diffusion and flow in two-dimensional systems. Biophys. J. 60:910–921.
59. Berglund, A. J. 2010. Statistics of camera-based single-particle tracking. Phys. Rev. E Stat. Nonlin. Soft Matter Phys. 82:011917.
60. Mobarak, E., M. Javanainen, . , I. Vattulainen. 2018. How to minimize dye-induced perturbations while studying biomembrane structure and dynamics: PEG linkers as a rational alternative. Biochim. Biophys. Acta. Biomembr. 1860:2436–2445.
61. Machán, R., and M. Hof. 2010. Lipid diffusion in planar membranes investigated by fluorescence correlation spectroscopy. Biochim. Biophys. Acta. 1798:1377–1391.
62. Kelly, C. V. 2022. Continuum-membrane-phase-curvature-simulation, GitHub. https://github.com/CVKellyWSU/Continuum-membrane-phase-curvature-simulation.
63. Sadeghi, S., M. Müller, and R. L. C. Vink. 2014. Raft formation in lipid bilayers coupled to curvature. Biophys. J. 107:1591–1600.
64. Rangamani, P. 2022. The many faces of membrane tension: challenges across systems and scales. Biochim. Biophys. Acta. Biomembr. 1864:183897.
65. Abraham, M. J., T. Murtola, . , E. Lindahl. 2015. GROMACS: high performance molecular simulations through multi-level parallelism from laptops to supercomputers. SoftwareX. 1–2:19–25.
66. Cino, E. A., and D. P. Tieleman. 2022. Curvature-based sorting of eight lipid types in asymmetric buckled plasma membrane models. Biophys. J. 121:2060–2068.
67. Javanainen, M. 2020. Simulations of POPC membranes of various shapes., Zenodo. 4196842. https://zenodo.org/record/4196842.
68. Javanainen, M., and B. Fabian. 2021. Ternary lipid composition in a curved geometry., Zenodo. 4445375. https://zenodo.org/record/4445375.
69. Veatch, S. L., K. Gawrisch, and S. L. Keller. 2006. Closed-loop miscibility gap and quantitative tie-lines in ternary membranes containing diphytanoyl PC. Biophys. J. 90:4428–4436.